microorganisms

MDPI

Article

Interaction between Illite and a *Pseudomonas stutzeri*-Heavy Oil Biodegradation Complex

Lei Li, Yun Yang Wan *, Hong Mei Mu, Sheng Bao Shi and Jian Fa Chen

State Key Laboratory of Petroleum Resources and Prospecting, Research Centre for Geomicrobial Resources and Application, Unconventional Petroleum Research Institute, College of Geosciences, China University of Petroleum, Beijing 102249, China

* Correspondence: wanyunyang@cup.edu.cn

Abstract: Illite is a widely distributed clay mineral with huge reserves in Earth's crust, but its effect on heavy oil biodegradation is rarely reported. This study made an investigation of the interactions between illite and a *Pseudomonas stutzeri*-heavy oil complex (*Pst*HO). Results showed that, although illite exerted a negative effect on *P. stutzeri* degrading heavy oil by inhibiting the biodegradation of 64 saturated hydrocarbons (SHs) and 50 aromatic hydrocarbons (AHs), it selectively stimulated the biodegradation of 45 AHs with a specific structure, and its biogenic kaolinization at room temperature (35 °C) and pressure (1 atm) was observed in *Pst*HO for the first time. The finding points out for the first time that, in *Pst*HO, illite may change the quasi-sequential of AHs biodegradation of heavy oil, as well as its kaolinization without clay intermediate.

Keywords: biodegradation; illite; *Pseudomonas stutzeri*; heavy oil; inhibition; stimulation

check for updates

Citation: Li, L.; Wan, Y.Y.; Mu, H.M.; Shi, S.B.; Chen, J.F. Interaction between Illite and a *Pseudomonas stutzeri*-Heavy Oil Biodegradation Complex. *Microorganisms* **2023**, *11*, 330. https://doi.org/10.3390/microorganisms11020330

Academic Editors: Tamara N. Nazina and Bo-Zhong Mu

Received: 29 November 2022
Revised: 11 January 2023
Accepted: 12 January 2023
Published: 28 January 2023

1. Introduction

Illite clay minerals account for more than half of the clay minerals in Earth's crust [1]. However, the majority of the studies on the effects of clay minerals on crude oil biodegradation by microorganisms have mainly focused on montmorillonite (Mon; for all abbreviations in this paper, see Table 1), kaolinite (Kao), saponite (Sap), palygorskite (Pal), vermiculite, and nontronite (Table 2). To the best of our knowledge, possibly because illite does not possess a remarkable specific surface area (SSA) [2], cation exchange capacity (CEC) [3], swelling property [4,5], and unique clay mineral microstructure [6], there are no reports on the effects of illite on crude oil biodegradation (Table 2), especially, biodegradation of heavy oil. Heavy oil is an important resource accounting for 21.3% of the global known recoverable oil resources [7]. As research on heavy oil biodegradation is difficult [8] due to the higher viscosity and density of heavy oil [9], there are only a few reports available on the influence of clay minerals on the biodegradation of heavy oil, except those affected by specific environmental conditions at a certain time (Table 2).

Most of the previous studies had focused on unidentified microbial community easily degradable crude oil systems (Table 2), and only a few identified microbial species were involved, such as Alcanivorax borkumensis and Pseudomonas aeruginosa (Table 2). The macro phenomenon of crude oil degradation by an unidentified microbial community is a sum of selective degradations of crude oil by all microorganisms in the microbial community and varies with the composition and abundance of microbial species in the microbial community [10,11], which is an obstacle to correctly understand the role of clay minerals in crude oil biodegradation. As a crude oil degrading bacterium [12–15], *Pseudomonas stutzeri* has been detected in heavy oil reservoirs [16]; however, there are no studies on heavy oil biodegradation by this bacterium, not to mention the influence of clay minerals.

The present study is the first to investigate the interaction between illite and a *P. stutzeri*-heavy oil biodegradation complex (*Pst*HO). The biodegradation of heavy oil by *P. stutzeri*

in the presence of illite was examined, and different effects of illite on the biodegradation of SHs and AHs compounds were determined. Furthermore, biogenic kaolinization of illite without smectite formation [17,18] in the illite-*Pst*HO was reported for the first time.

Table 1. Abbreviation list for this paper.

No.	First Appearance Location	Content	Abbreviation	Occurrence Number
1	Introduction	montmorillonite	Mon	8
2		kaolinite	Kao	12
3		saponite	Sap	5
4		palygorskite	Pal	5
5		specific surface area	SSA	10
6		cation exchange capacity	CEC	9
7		*Pseudomonas stutzeri*-heavy oil system	*Pst*HO	25
8		saturated hydrocarbons	SHs	35
9		aromatic hydrocarbons	AHs	46
10	Materials and methods	modified Van Niel culture medium	MVN	16
11		gas chromatography	GC	5
12		conductivity	σ	9
13		redox potential	Eh	9
14		resins	Rs	4
15		asphaltenes	Aps	4
16		saturated hydrocarbons, aromatic hydrocarbons, resins, and asphaltenes	SARA	6
17		gas chromatography–mass spectrometry	GC–MS	8
18		X-ray diffraction	XRD	3
19		scanning electron microscope	SEM	4
20		fraction content	FC	3
21		the content difference of CO_2, O_2 and N_2 between illite-*Pst*HO and atmosphere	ΔG	3
22		residual mass content	*RMC*	11
23		degradation rate	*DR*	4
24		influence degree	*IND*	9
25	Results and discussion	Peters and Moldowan	PM	2
26		high ring number (≥4) aromatic hydrocarbons	HRAHs	7
27	Supplemental Materials	8 g illite	Ill-8	29
28		32 g illite	Ill-32	29
29		organic modified montmorillonite	Mon-Org	18
30		acid modified montmorillonite	Mon-Acid	29
31		sodium ion modified montmorillonite	Mon-Na	10
32		potassium ion modified montmorillonite	Mon-K	21
33		calcium ion modified montmorillonite	Mon-Ca	21
34		iron ion modified montmorillonite	Mon-Fe	21
35		acid modified palygorskite	Pal-Acid	10
36		acid modified saponite	Sap-Acid	8
37		organic modified saponite	Sap-Org	3
38		acid modified kaolinite	Kao-Acid	8
39		magnesium ion modified montmorillonite	Mon-Mg	8
40		zinc ion modified montmorillonite	Mon-Zn	9
41		aluminum ion modified montmorillonite	Mon-Al	8
42		chromium ion modified montmorillonite	Mon-Cr	9

Note: In order of appearance in the context.

Table 2. Effect of clay minerals on microbial degradation of petroleum hydrocarbons.

No.	Clay Mineral	Clay Source/ Treatment Method	Degradation Duration [1]	Substrate	Effect	Mechanism of Influence	Aerobic/Anaerobic	Degrader	Reference
1	Mix	Collected	56 d	Crude oil	Stimulation for SHs, Neutral for AHs	Increase biological accessibility	Aerobic	Microbial community	[19]
2	Kao	Purchased	24 d	Heavy oil in the environment	Stimulation	C-O-Na-Si stimulates metabolism	Aerobic	Microbial community	[20]
3	Mon Kao	Collected	105 d	Heavy oil in the environment	Stimulation	Stimulate growth and buffer pH	Aerobic	*Pseudomonas aeruginosa* + Microbial community	[21]
4	Mon Mon Kao-low Kao-high	Collected	36 mon	Heavy oil in the environment	Stimulation Stimulation Stimulation Overall inhibition, inhibition for SHs and AHs, stimulation for Rs and As	Stimulate growth and buffer pH, C-O-Na-Si stimulates metabolism Low SSA and CEC	Aerobic	Microbial community	[22]
5	Ver	Purchased	20 d	Naphthalene, Anthracene	Stimulation	Protect from toxicity	Aerobic	Microbial community	[23]
6	Mon Mon-Org Mon-Acid Mon-Na Mon-K Mon-Ca Mon-Fe	Purchased Modified by DDDMA bromide HCl modified NaCl modified KCl modified $CaCl_2$ modified $FeCl_3$ modified	60 d	Crude oil	Stimulation Neutral Neutral Stimulation Neutral Stimulation Stimulation	Adsorbent Poor adsorption Poor adsorption Adsorbent Poor adsorption Poor adsorption Poor adsorption	Aerobic + Anaerobic	Microbial community	[24]

Table 2. *Cont.*

No.	Clay Mineral	Clay Source/ Treatment Method	Degradation Duration [1]	Substrate	Effect	Mechanism of Influence	Aerobic/Anaerobic	Degrader	Reference
7	Mon	Purchased	21 d	SHs in crude oil	Stimulation	High SSA	Aerobic + Anaerobic	Microbial community	[25]
	Mon-Acid	HCl modified			Inhibition	Low pH			
	Mon-Org	DDDMA bromide modified			Inhibition	Adsorption is blocked and local bridging effect are weakened			
	Pal	Collected			Stimulation	High SSA			
	Pal-Acid	HCl modified			Inhibition	Low pH			
	Sap	Collected			Neutral	/			
	Sap-Acid	HCl modified			Inhibition	Low pH			
	Sap-Org	DDDMA bromide modified			Inhibition	/			
	Kao	Purchased			Inhibition	No local bridging effect, Low SSA			
	Kao-Acid	HCl modified			Inhibition	Low pH			
8	Mon-Na	Purchased	60 d	Crude oil	Stimulation	High SSA and CEC	Aerobic + Anaerobic	Microbial community	[26]
	Mon-Org	Modified by DDDMA bromide			Inhibition	Hydrophobicity			
	Sap	Collected			Stimulation	High SSA and CEC			
	Sap-Org	Modified by DDDMA bromide			Neutral	Hydrophobicity			
9	Kao	Purchased	60 d	Crude oil	Inhibition	Low SSA and CEC	Aerobic + Anaerobic	Microbial community	[27]
	Pal	Collected			Stimulation	High SSA and CEC			
	Sap	Collected			Neutral	/			
	Mon	Purchased			Stimulation	High SSA and CEC			
	Kao-Acid	HCl modified			Inhibition	Reduce pH to form biological toxicity			
	Pal-Acid	HCl modified			Inhibition				
	Sap-Acid	HCl modified			Inhibition				
	Mon-Acid	HCl modified			Inhibition				

Table 2. *Cont.*

No.	Clay Mineral	Clay Source/ Treatment Method	Degradation Duration [1]	Substrate	Effect	Mechanism of Influence	Aerobic/Anaerobic	Degrader	Reference
10	Mon	Purchased	60 d	Crude oil	Stimulation	/	Aerobic + Anaerobic	Microbial community	[28]
	Mon-Na	NaCl modified			Stimulation	SSA, CEC			
	Mon-K	KCl modified			Inhibition	Adsorbent			
	Mon-Mg	$MgCl_2$ modified			/	/			
	Mon-Ca	$CaCl_2$ modified			Stimulation	SSA, CEC			
	Mon-Zn	$ZnCl_2$ modified			Inhibition	Adsorbent			
	Mon-Al	$AlCl_3$ modified			Inhibition	Increase acidity			
	Mon-Cr	$CrCl_3$ modified			Inhibition	Adsorb and increase acidity			
	Mon-Fe	$FeCl_3$ modified			Stimulation	CEC			
11	Mon	Purchased	60 d	Phenanthrene and dibenzothiophene compounds	Stimulation	/	Aerobic + Anaerobic	Microbial community	[29]
	Mon-Acid	HCl modified			Inhibition				
	Mon-Org	Modified by DDDMA bromide			Stimulation				
	Mon-Na	NaCl modified			Stimulation				
	Mon-K	KCl modified			Inhibition				
	Mon-Ca	$CaCl_2$ modified			Stimulation				
	Mon-Zn	$ZnCl_2$ modified			Inhibition				
	Mon-Cr	$CrCl_3$ modified			Inhibition				
	Mon-Fe	$FeCl_3$ modified			Stimulation				

Table 2. *Cont.*

No.	Clay Mineral	Clay Source/ Treatment Method	Degradation Duration [1]	Substrate	Effect	Mechanism of Influence	Aerobic/Anaerobic	Degrader	Reference
12	Mon-Na	NaCl modified	60 d	AHs in crude oil	Stimulation	SSA, CEC	Aerobic	Microbial community	[30]
	Mon-K	KCl modified			Inhibition	Adsorption and hydrophobic siloxane surface exposure			
	Mon-Mg	$MgCl_2$ modified			Stimulation	High SSA and CEC, Local bridging effect			
	Mon-Ca	$CaCl_2$ modified			Stimulation	SSA, CEC and local bridging effect			
	Mon-Zn	$ZnCl_2$ modified			Inhibition	Adsorbed aromatic hydrocarbons			
	Mon-Al	$AlCl_3$ modified			Inhibition	Low SSA			
	Mon-Cr	$CrCl_3$ modified			Inhibition	Low SSA			
	Mon-Fe	$FeCl_3$ modified			Stimulation	High SSA			
13	Bentonite-Surf + Acid	Surfactant and palmitic acid modified	21 d	Phenanthrene and cadmium contaminated soil	Stimulation	Adsorb cadmium to reduce toxicity	Aerobic	Microbial community	[31]
	Bentonite-Surf	Surfactant modified			Stimulation				
	Bentonite	Purchased			Stimulation				
14	Calcium bentonite	Collected	30 d/60 d	Crude oil in the environment	Stimulation	High SSA	Aerobic + Anaerobic	Microbial community	[32]
	Fuller soil	Collected			Stimulation				
	Kao	Collected			Stimulation				
	Eutrophic bentonite	Mixed with nutrients containing nitrogen, phosphorus and potassium			Stimulation				
	Eutrophic fuller soil				Stimulation	Fixed nutrients			
	Eutrophic kaolinite				Stimulation				

Table 2. *Cont.*

No.	Clay Mineral	Clay Source/ Treatment Method	Degradation Duration [1]	Substrate	Effect	Mechanism of Influence	Aerobic/Anaerobic	Degrader	Reference
15	Pal	Purchased	5 d	Phenanthrene(C^{14})	Stimulation	Stimulate biofilm formation and accommodate extracellular enzymes	Aerobic	*Burkholderia sartisoli*	[33]
	Pal-Ther	Thermal modification			Stimulation	Reduced cooperation with the phenanthrene			
16	Mon	Collected	21 d	Phenanthrene(C^{14})	Stimulation	High SSA and CEC	Aerobic	*Burkholderia sartisoli* RP007 + Microbial community	[34]
	Mon-Acid	HCl modified			Stimulation	Element release, increase SSA and CEC			
	Mon-Alk	NaOH modified			Stimulation				
	Pal	Purchased			Stimulation	High SSA and CEC			
	Pal-Acid	HCl modified			Stimulation	Element release, increase SSA and CEC			
	Pal-Alk	NaOH modified			Stimulation				
17	Mon	Purchased	/	Crude oil	Stimulation	Stimulate contact with nutrients	Aerobic + Anaerobic	Microbial community	[35]
	Sap	Collected			Stimulation	Increase nutrient utilization			
	Mon-Org	Modified by didecyl dimethyl ammonium bromide			Inhibition for LMW AHs	Adsorbent			
	Sap-Org				Inhibition for LMW AHs and stimulation for phenanthrene	Adsorbent			
18	Mon	Purchased	21 d	AHs in crude oil	Stimulation	High SSA and CEC	Aerobic + Anaerobic	Microbial community	[36]
	Sap	Collected			Stimulation				
	Pal	Purchased			Stimulation	Channel structure			
	Kao	Purchased			Inhibition	Influence of impurities			
	Mon-Acid	HCl modified			Inhibition				
	Sap-Acid	HCl modified			Inhibition	Decrease pH			
	Pal-Acid	HCl modified			Inhibition				
	Kao-Acid	HCl modified			Inhibition				
19	Kao	Purchased	48 h	Phenanthrene	Stimulation	Silicon/oxygen atoms stimulate biological effects	Aerobic	*Sphingomonas* sp. GY2B	[37]
	Quartz	Purchased			Stimulation				

Table 2. *Cont.*

No.	Clay Mineral	Clay Source/ Treatment Method	Degradation Duration [1]	Substrate	Effect	Mechanism of Influence	Aerobic/Anaerobic	Degrader	Reference
20	Nontronite	Collected	37 d	Crude oil	Stimulation	Stimulate ion exchange and nutrient absorption	Aerobic	*Alcanivorax borkumensis*	[38]
21	Bentonite	Purchased	70 d	AHs and cadmium contaminated soil	Stimulation	Adsorption of heavy metals	Aerobic + Anaerobic	Microbial community	[39]
	Bentonite-Surf	Modified by Arquad			Stimulation	Improve biological activity			
	Bentonite-Surf + Acid	Modified by Arquad and palmitic acid			Stimulation	Adsorb cadmium to reduce toxicity			
22	Pal	Collected	2 mon	Crude oil contaminated soil	Neutral	/	Aerobic	Microbial community	[40]
	Pal-Org	Modified by DDTMA bromide			Neutral				
23	Illite	Purchased	56 d	Heavy oil	Inhibition for all SHs and 50 AHs, stimulation for 45 AHs	Adsorption and cation-π	Aerobic	*Pseudomonas stutzeri*	This study

Note: Kao-low is low defect kaolinite; Kao-high is high defect kaolinite; Bentonite-Surf + Acid is surfactant and acid modified bentonite; Bentonite-Surf is surfactant modified bentonite; Pal-Ther is thermal modification palygorskite; Mon-Alk is alkali modified montmorillonite; Pal-Alk is alkali modified palygorskite; Pal-Org is organically modified palygorskite; DDDMA is didecyldimethylammonium; DDTMA is dodecyltrimethylammonium; LMW is low molecular weight. See Table 1 for the other abbreviations; [1]. h stands for hour, d stands for day, mon stands for month; / Indicates that there is no relevant information in the literature.

2. Materials and Methods

2.1. Materials

2.1.1. Illite

Illite (Chengde, China) was purchased from Tianjin Guangfu Co. Ltd., Tianjin, China. According to Wang's research [41], the composition of illite from Chengde is: 53.5% SiO_2; 27.67% Al_2O_3; 1.14% Fe_2O_3; 0.036% FeO;1.25% MgO; 0.64% CaO; 0.75% Na_2O; 7.77% K_2O, and 5.25% loss-on-ignition (LOI). This natural illite clay is initially a wet mud cake without particle size screening, and its CEC is 140 meq/kg [4].

2.1.2. Strain *Pseudomonas stutzeri* L1SHX-3X

Aerobic *P. stutzeri* strain L1SHX-3X was isolated from a heavy oil–water mixture of the production well in Liaohe Oil Field, China, and was identified [42,43] by the Research Centre for Geomicrobial Resources and Application, China University of Petroleum, Beijing, China. The strain was preserved by converting it into freeze-dried powder [44] and stored in a refrigerator (Thermo Fisher Scientific, Waltham, MA, USA) at −80 °C.

2.1.3. Heavy Oil

The heavy oil L1YJC23 used in this study was collected from JC23 well in the Jin 45 Block of Liaohe Oil Field and preserved in an airtight plastic bucket [42].

All the chemical agents were of analytical grade and supplied by Tianjin Fuchen Chemical Reagents Factory, Tianjin, China.

2.2. Methods

2.2.1. Experiment on the Interaction between Illite and *P. stutzeri*-Heavy Oil Complex

Illite was sifted through a 200-mesh sieve (74 μm) and dried in an oven (75 °C, 48 h), and its particle size and SSA were measured.

Reactivation of *P. stutzeri* was achieved by adding 1 mL of freeze-dried powder of *P. stutzeri* (obtained with 500 mL of *P. stutzeri* L1SHX-3X culture medium in logarithmic growth stage) to 4 mL of modified Van Niel culture medium [45] (MVN-R) under sterile conditions and incubating in a shaker (120 rpm, 35 °C) for 2 days [44]. The MVN-R contained 4.50 g/L $C_6H_{12}O_6$, 0.10 g/L of NH_4Cl, 0.04 g/L of $MgCl_2{\cdot}6H_2O$, 0.05 g/L of KH_2PO_4, 0.50 g/L of Na_2CO_3, 0.10 g/L of $Na_2S{\cdot}9H_2O$, and 0.10 g/L of NaCl. After 2 days of incubation, 4 mL of the culture were mixed with 40 mL MVN-R under the same culture conditions [44] until *P. stutzeri* concentration reached 10^8 cell/mL under an Eclipse Ni-U upright microscope (Nikon, Tokyo, Japan) (Figure S1) for standby.

Before starting the experiment, the viscosity and density of heavy oil were measured, and the genes of in situ microorganisms in heavy oil were analyzed. In order not to affect the composition of the heavy oil, it was not sterilized.

The illite and MVN were first placed in 250 mL conical flasks (Table 3). The MVN was consistent with MVN-R except that it contained no $C_6H_{12}O_6$. Then, the flasks were sealed with high-temperature resistant sealing films (BKMAN, Shanghai, China), and placed in a sterilizer (Zealway, Wilmington, DE, USA) for 20 min (121 °C, 1 atm). Then, *P. stutzeri* culture medium and heavy oil were added into the conical flasks under sterile conditions, and the flasks were sealed using Parafilm® sealing film (Bemis, Neenah, WI, USA), which is germproof and breathable (150 cm^3/m^2/24 h at 22.78 °C for O_2). All the flasks were incubated in a shaker (STIK, Shanghai, China) at 35 °C, 120 rpmfor 56 days.

A total of five groups of illite-*Pst*HO experiments were established (Table 3). The control groups, P0I0, and P0I8 were used to determine the effects of MVN and illite on heavy oil without *P. stutzeri* (Table 3). The experimental groups, P2I0, P2I8, and P2I32, contained the constant volume of *P. stutzeri* culture medium and different masses of illite (Table 3) to determine the effect of illite content. P2I8 and P2I32 contained 8 and 32 g of illite, respectively, simulating two environmental conditions with different solid contents (15.8% and 43.0%, respectively) and partly representing marine sedimentary and humid

soil [22,39], respectively. Three parallel replicates were established for each group (Table 3) for error analysis.

Table 3. Experimental setup of the illite-*Pst*HO.

Group [#]	Volume of *P. stutzeri* Culture (mL)	Optical Density of Culture (Cell/mL)	Mass of Illite (g)	Mass of Heavy Oil (g)	Volume of MVN (mL)	Duration (d)	Number of Parallel Replicates
P0I0	0	10^8	0	0.50	40.0	56	3
P0I8	0		8.00				
P2I0	2.0		0.00				
P2I8	2.0		8.00				
P2I32	2.0		32.00				

Note: See Table 1 for *Pst*HO and MVN. [#]. P represents *P. stutzeri*, followed by 0 or 2, which denotes the volume of *P. stutzeri* culture; I indicates illite, followed by 0, 8, or 32, which shows the mass of illite.

After 56 days, gas samples were collected from the conical flask by piercing the sealing film with a syringe and analyzed by gas chromatography (GC). The contents of the conical flask were filtered using 2-μm filter paper to obtain liquid and illite-heavy oil mixtures. The pH, conductivity (σ), and redox potential (Eh) of the liquid were determined, and the illite-heavy oil mixtures were mixed with 50 mL of organic solvent mixture (C_6H_{14} and C_3H_6O at a ratio of 1:4) [46] and subjected to ultrasonication (60 min, 45 °C) to extract heavy oil. Further, heavy oil extraction was performed using solvent CH_2Cl_2 until CH_2Cl_2 leachate had no absorption in the spectral range of 200–400 nm on an ultraviolet-visible spectrophotometer (Varian Cary 100 UV-Vis, Agilent, Santa Clara, CA, USA) [47]. The heavy oil dissolved in an organic solvent mixture, and CH_2Cl_2 was collected and concentrated to 4 mL using a rotary evaporator (Yarong, Qingdao, China) at 65 °C, and then, further dried at room temperature (24 °C) to a constant weight [47] (weighed every 4 h, with differences of three consecutive measurements maintained within 0.0010 g) to obtain heavy oil [47]. Fractions analysis of SHs, AHs, resins (Rs), and asphaltenes (Aps) (SARA) in heavy oil [48] was performed, and the fractions of SHs and AHs were subjected to gas chromatography–mass spectrometry (GC–MS). Illite with CH_2Cl_2 was dried in an oven at 75 °C to a constant weight (as described previously) and further analyzed by X-ray diffraction (XRD) and scanning electron microscopy (SEM).

2.2.2. Measurements of Particle Size and SSA of Illite

To measure the particle size and SSA of illite, 2 g of illite was mixed with deionized water dispersant and examined under a blue light source with a 466 nm wavelength on a Mastersizer 3000 (Malvern Panalytical, Great Malvern, UK) [49]. The measurement was performed in triplicate, and the average value was determined.

2.2.3. Measurements of Viscosity and Density of Heavy Oil

To measure the viscosity of heavy oil, a BS/U tube viscometer (Cannon, Huntington, NY, USA) loaded with heavy oil L1YJC23 was vertically placed into a constant-temperature water bath at 40 °C for 20 min. The time when the heavy oil reached the specific liquid level was recorded to obtain the viscosity [50].

To determine the density of heavy oil, the test temperature was set to 20 °C, and the heavy oil was injected into the U-shaped pipe of the digital density meter (DMA 4501, Anton Paar, Graz, Austria) using a syringe [51].

Measurements of viscosity and density of heavy oil were performed in triplicates individually, and the average values were obtained.

2.2.4. Gene Sequence Analysis of In Situ Microorganisms in Heavy Oil

Biomass from heavy oil L1YJC23 was extracted with isooctane, and the deoxyribonucleic acid was extracted from the biomass using Fast DNA Spin Kit (MP Biomed-

ical, Irvine, California, USA) [42]. The genes were sequenced on a MiSeq™ System (Illumina, San Diego, CA, USA) and analyzed using Galaxy Platform [42,43,52] (https://galaxyproject.org/, accessed on 19 January 2022).

2.2.5. Gas Chromatography Analysis

10.0 mL of gas samples from the illite-*Pst*HO flasks and atmosphere were employed for GC analysis (Agilent HP-6890A, Agilent, Santa Clara, CA, USA). The capillary column was HP-5 (30 m × 0.32 mm, 5% phenyl methyl siloxane), carrier gas was He (99.99%), power gas was N_2 (99.99%), and temperatures of the oven, front sample cell, front detector, and back detector were 50 °C, 100 °C, 200 °C, and 200 °C, respectively [53].

The differences in CO_2, O_2, and N_2 contents between the gas samples from the illite-*Pst*HO flasks and atmosphere (ΔG, %) were calculated using the following Equation (1):

$$\Delta G = G_a - G^* \quad (1)$$

where G_a is the percentage content of CO_2, O_2, or N_2 in gas from the illite-*Pst*HO (%) experiment and G^* is the percentage content of CO_2, O_2, or N_2 in the atmosphere (%).

2.2.6. Measurements of pH, Conductivity, and Redox Potential

The pH, σ, and Eh of the MVN and illite-*Pst*HO were measured using three probes (Inlab Expert Pro pH, Inlab Redox, and Inlab 731, respectively) on a Mettler Toledo Seven-Multi™ (Mettler Toledo, Columbus, OH, USA) [53].

2.2.7. Fractions Analysis of Heavy Oil

SARA analysis separates heavy oil components according to their polarizability and polarity by column chromatography [54]. In the present study, 30 mL n-hexane was added to 20.0–50.0 mg of heavy oil, and the Aps were filtered out with absorbent cotton after ultrasonication (5 min). The SHs, AHs, and Rs were obtained by using a chromatographic column (4 g of silica gel and 3 g of activated alumina) with n-hexane, dichloromethane, and ethanol [47,55].

The fraction content (*FC*, %) of SARA was calculated using the following Equation (2):

$$FC = \frac{M_e}{M} \times 100\% \quad (2)$$

where M_e is the mass of each SARA in heavy oil L1YJC23 or illite-*Pst*HO (g) and M is the mass of heavy oil L1YJC23 used in each group (0.5 g).

2.2.8. Gas Chromatography–Mass Spectrometry Analysis of Saturated and Aromatic Hydrocarbons

The compounds in the SHs and AHs of the heavy oil were characterized and quantified by GC–MS. Deuterated tetracosane (D_{50}-$n$$C_{24}$, 10 μg) and deuterated dibenzothiophene (D-substituted dibenzthiophene, 10 μg) were used as internal standards for SHs and AHs, respectively. Trace-DSQ mass spectrometer (Thermo Finnigan, San Jose, CA, USA) coupled to an HP 6890 gas chromatograph (Agilent, Santa Clara, CA, USA) was used for GC–MS analysis. The column was HP-5MS (30 m × 0.25 mm, ID) with a 0.25-μm coating, and He (99.99%) was used as the carrier gas. The oven temperature of the gas chromatograph was initially set to 50 °C and was, subsequently, increased to 120 °C at a rate of 20 °C/min, 250 °C at a rate of 4 °C/min, and 310 °C at a rate of 3 °C/min and maintained for 30 min. The mass spectrometer was operated in full-scan electron impact mode with an electron energy of 70 eV [56].

The residual mass content (*RMC*) of the SHs and AHs in the heavy oil L1YJC23 or illite-*Pst*HO was obtained by GC–MS. The *RMC* (μg/g), the degradation rate of heavy oil

by *P. stutzeri* (*DR*, %), and the influence degree (*IND*, %) of illite on biodegradation were calculated using the following Equations (3)–(5):

$$RMC = k\frac{S_a m^*}{S^* m_a} \tag{3}$$

$$DR = \frac{M^* - M_p}{M^*} \times 100\% \tag{4}$$

$$IND = (\frac{M^* - M_{ip}}{M^*} - \frac{M^* - M_{op}}{M^*}) \times 100\% \tag{5}$$

where k is the response coefficient, S_a is the peak area of each compound in SHs and AHs, S^* is the peak area of the internal standard, m^* is the mass of the internal standard (10 μg), m_a is the mass of heavy oil used in fractionation (g), M^* is the *RMC* of each compound of SHs or AHs in heavy oil L1YJC23 (μg/g), M_p is the *RMC* of each compound of SHs or AHs in P2I0, P2I8, or P2I32 with *P. stutzeri* (μg/g), M_{ip} is the *RMC* of each compound of SHs or AHs in P2I8 and P2I32 with illite clay and *P. stutzeri* (μg/g), and M_{op} is the *RMC* of each compound in SHs or AHs in P2I0 without illite and with *P. stutzeri* (μg/g). To facilitate comparison with previous studies, the *IND* of other clay minerals on biodegradation was calculated based on Equation (5).

In order to support the scientific and responsible biochemical processes [57] in the illite-*Pst*HO, mass balance and stoichiometry were performed in the data-checking process using the following Equations (6) and (7):

$$M{\cdot}FC_{SHs} = \frac{m_a}{k} \cdot \sum_{i=1}^{64} RMC_{SH}{\cdot}10^{-6} \tag{6}$$

$$M{\cdot}FC_{AHs} = \frac{m_a}{k} \cdot \sum_{i=1}^{96} RMC_{AH}{\cdot}10^{-6} \tag{7}$$

where FC_{SHs} is the fraction content of SHs (%), RMC_{SH} is the *RMC* of each compound in SHs (μg/g), FC_{AHs} is the fraction content of AHs (%), and RMC_{AH} is the *RMC* of each compound in AHs (μg/g).

2.2.9. X-ray Diffraction Analysis of Illite

XRD analysis of illite was performed using D8 Advance X-ray diffractometer (Bruker, Billerica, MA, USA). The tube voltage was 40 kV and the tube current was 25 mA [53].

2.2.10. Scanning Electron Microscopy Analysis of Illite

The illite was sprayed with gold and observed using TESCAN VEGA 3 (Czech, TESCAN, Brno, Czech Republic) SEM with an electron detector at an accelerating voltage of 20 kV [53].

3. Results and Discussion

3.1. Effect of Illite on Heavy Oil and In Situ Microorganisms in Heavy Oil

Illite was incapable of altering the SARA fractions of heavy oil in the absence of *P. stutzeri*; however, it modified the existing state of heavy oil. In this study, the recovery efficiency of eluted SARA fractions ranged from 90% to 99%, completely meeting the requirements for its effectiveness (85–115%) [58]. The SARA fractions of P0I0, P0I8, and heavy oil L1YJC23 were consistent (Figure 1). Due to its high viscosity (1967 MPa·s) and density (0.949 g/cm^3), heavy oil remained suspended and dispersed in the MVN as droplets of different sizes or adhered to the inner wall of the conical flask in the absence of illite. However, the adsorption of illite particles (8.67 μm; Figure S2) caused the aggregation of oil droplets and the formation of larger illite-heavy oil mixtures. The mixtures were mostly covered with illite due to the relative excess proportion of illite (8/32 g) to heavy oil (0.5 g).

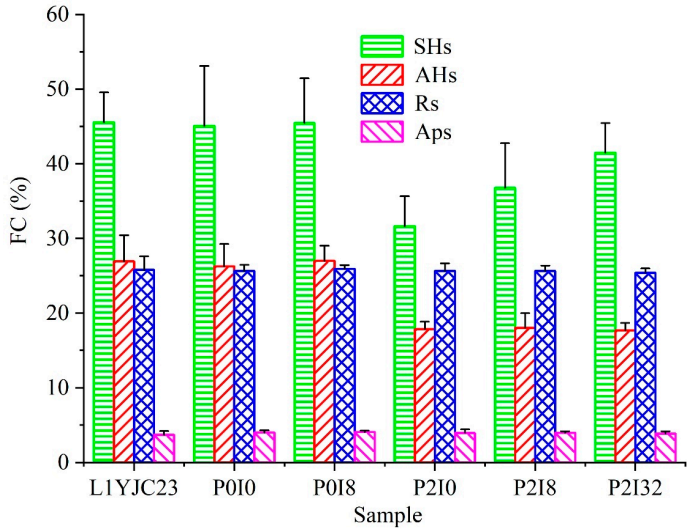

Figure 1. SARA analysis of heavy oil L1YJC23 and illite-*Pst*HO. Note: FC is fraction content; SHs, AHs, Rs, and Aps are saturated hydrocarbons, aromatic hydrocarbons, resins, and asphaltenes, respectively; see Table 3 for P0I0, P0I8, P2I0, P2I8, and P2I32.

Illite did not affect the activity of in situ microorganisms in heavy oil. The gene sequence analysis indicated that the in situ microorganisms in heavy oil L1YJC23 included 61.1% aerobic and 14.1% facultative anaerobic microorganisms (anaerobic and unidentified microorganisms accounted for 17.1% and 7.7%, respectively) (Figure S3). Among the in situ microorganisms in heavy oil, Pseudomonas was the dominant genus with the largest number of reads (20.1%, Figure S3). Aerobic and facultative anaerobic microorganisms (Figure S3) activated by MVN consumed O_2 and produced CO_2, which resulted in gas content differences of CO_2 and O_2 between groups of P0I0 and P0I8 without *P. stutzeri* and atmosphere (Figure S4). Comparison of P0I0 with P0I8 revealed that the addition of 8 g of illite did not cause any changes in the CO_2 and O_2 contents (Figure S4), indicating that illite did not affect the activity of in situ microorganisms in heavy oil L1YJC23. Moreover, in situ microorganisms did not alter the SARA fractions of heavy oil, irrespective of the presence or absence of illite (Figure 1).

3.2. Illite Effect on P. stutzeri-Heavy Oil Complex

3.2.1. Illite Effect on Activity of *P. stutzeri*

Illite slightly inhibited the activity of *P. stutzeri*. In the absence of illite, P2I0 presented the highest CO_2 and lowest O_2 contents (Figure S4) due to the metabolism of the aerobic bacterium *P. stutzeri* [12]. The pH, σ, and Eh of P2I0 were the lowest (Table S1) because of the consumption of inorganic salts, O_2, and petroleum hydrocarbons by *P. stutzeri* to produce CO_2 and acidic compounds [12]. Consequently, P2I0 also showed the highest *DR* (23.0%) for heavy oil, followed by P2I8 (17.9%) and P2I32 (13.2%) (Figure 1). Comparison of P2I0, P2I8, and P2I32 revealed that the presence of illite reduced the CO_2 content, increased the O_2 content (Figure S4), reduced the changes in pH, σ, and Eh (Table S1), and decreased *DR* (Figure 1). These results proved that illite had a negative effect on the activity of *P. stutzeri*, and the degree of the effect was positively related to the illite content (Figures 1 and S4; Table S1). However, the differences in the parameters (O_2 content < 1%, CO_2 content < 0.19%, pH < 1.5%, σ < 5.8%, Eh < 13.5%, and SHs fraction content < 9.8%; Figures 1 and S4; Table S1) were not sufficiently large to confirm any effect of illite on the metabolic pathways of *P. stutzeri*.

The slight inhibitory effect of illite on the activity of *P. stutzeri* might have been caused by a decrease in the bioaccessibility of heavy oil due to adsorption onto illite [59]. Illite was more likely to adsorb heavy oil droplets [60] than *P. stutzeri* [61] because both illite and *P. stutzeri* have negatively charged surfaces [12,22], and the excess illite coated the

surface of the heavy oil and formed a barrier against *P. stutzeri*. In contrast, the moderate SSA (1.294 m^2/g) and CEC [3] (140 meq/kg [4]) of illite were insufficient to elicit a positive effect on microbial activity similar to that of Kao with low SSA and CEC [22,25,27,36].

3.2.2. Illite Inhibition of Saturated Hydrocarbons Biodegradation

The GC–MS results revealed that illite inhibited the biodegradation of all 64 SHs in heavy oil L1YJC23 (Table S2 and Figure S5). Hopane was degraded without the formation of 25-norhopane (Table S2; Figures S5 and S6), indicating that the biodegradation level of heavy oil L1YJC23 was 7–8 on the Peters and Moldowan (PM) scale [8]. Furthermore, all n-alkane, alkyl cyclohexane, and isoprenoid components which should have been in the SHs of crude oil, were missing (Table S2; Figures S5 and S6). The *RMC* of all the 64 SHs showed a trend of P2I0 < P2I8 < P2I32 (Figure S5), indicating that the *IND* of illite was positively correlated with its content. In SHs with content >70 μg/g, the *DR* of *P. stutzeri* without illite were related to the molecular weight (Figure 2). A higher molecular weight usually denotes stronger biodegradation resistance [62,63], thus leading to lower *DR*. The inhibition of illite on the biodegradation of SHs in heavy oil can be a positive protective way during microbial-enhanced oil recovery processes [53].

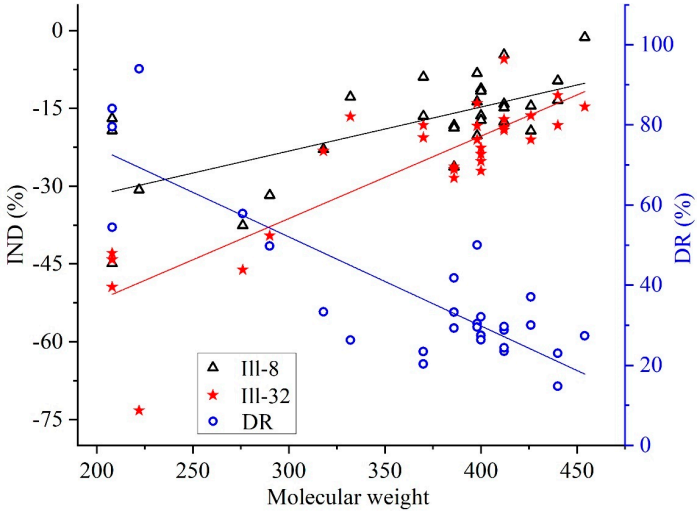

Figure 2. Relationship among the *IND* of illite, *DR* of *P. stutzeri* without illite, and molecular weight of SHs (content > 70 μg/g) in the illite-*Pst*HO. Note: *IND* is influence degree; *DR* is degradation rate; Ill-8 and Ill-32 represent 8 g and 32 g illite, respectively.

The adsorption of illite on SHs reduced their bioaccessibility, which was the main reason for the negative effect of illite. However, with an increase in the molecular weight of SHs, the adsorption of illite on SHs weakened, and the degree of reduction in bioaccessibility decreased, which led to a decrease in the inhibitory effect of illite (Figure 2). Generally, clay minerals with high SSA and CEC, such as Mon, Sap, and Pal, can stimulate biodegradation of SHs [25] (Figure S7); however, Kao and illite do not possess these properties, and hence, exert a negative effect on SHs biodegradation (Figure S7). Furthermore, the interlayer of illite does not contain divalent cations [60], and the positive effect of the local bridging effect [22,24–30,61] formed by the low concentration of divalent cations (Mg^{2+}, 7.87×10^{-6} mol) provided by MVN was weak, which was not sufficient to alter the inhibition caused by adsorption.

3.2.3. Two Effects of Illite on Aromatic Hydrocarbons Biodegradation

A total of 96 AHs were detected in the heavy oil L1YJC23 by GC–MS (Table S3, Figures 3 and S8), and were classified into five categories for ease of discussion, namely, naphthalene/phenanthrene/fluorene/biphenyl series and high-ring number (≥4) aromatic hydrocarbons (HRAHs) (Figures S9–S13). The degradation rate of AHs by *P. stutzeri* was not affected by illite (Figure 1); however, the GC–MS results of AHs suggested that illite might

have diverse effects on different AHs compounds (Figures S9–S13). After the verification of fractions and GC–MS data in mass balance and stoichiometry (Equations (6) and (7)), we found that illite inhibited the biodegradation of 50 AHs, stimulated the biodegradation of 45 AHs, and had no obvious effect on biphenyl (Bph, see Table S3 for the abbreviations of AHs used in this study) (Figure S12).

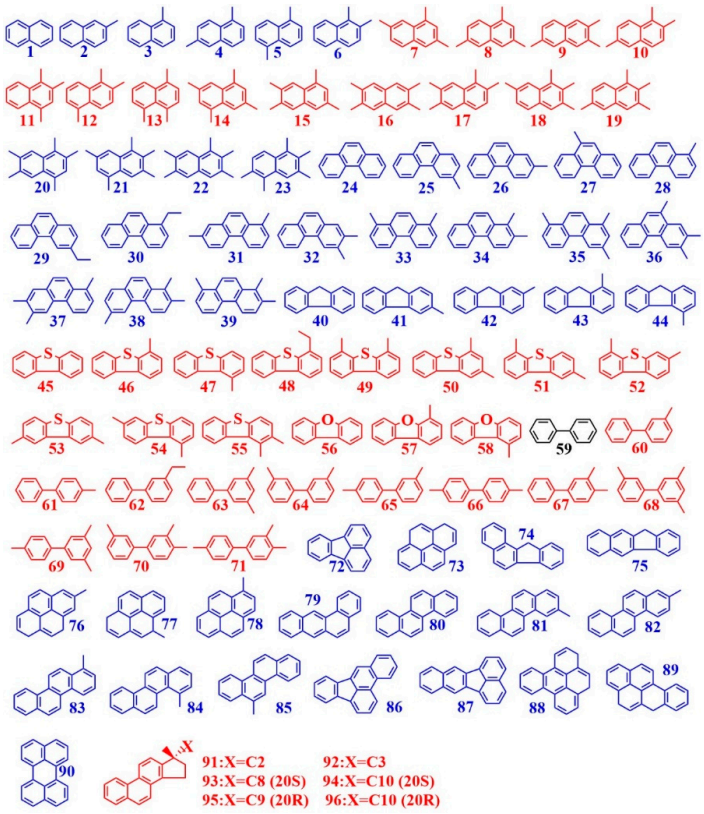

Figure 3. Molecular structures of AHs in heavy oil L1YJC23. Note: See Table S3 for No. of the AHs; blue, red, and black represent inhibition, stimulation, and uncertain effects of illite, respectively.

The effect of illite on the biodegradation of AHs in *Pst*HO was affected by the number of aromatic rings, and illite appeared to inhibit the biodegradation of AHs with a high number of aromatic rings. For example, although both trimethyl naphthalene (TMN) and trimethyl phenanthrene (TMP) have three methyl groups (Figure 3), illite stimulated TMN biodegradation (Figure S9) but inhibited TMP biodegradation (Figure S10), which may have been caused by the addition of an aromatic ring. Furthermore, monomethyl biphenyl (MeBph), monomethyl pyrene (MePyr), and monomethyl chrysene (MeChr) have one methyl substituent (Figure 3); illite also stimulated MeBph biodegradation (Figure S12) with two aromatic rings and inhibited biodegradation of MePyr and MeChr (Figure S13) with four aromatic rings. The more fused the rings of AHs, the stronger the ability of the compounds to resist biodegradation [64], with illite being more inclined to inhibit their biodegradation.

The effect of illite on the biodegradation of AHs in *Pst*HO was affected by the number of methyl substituents. In the two-ring naphthalene series (Figure 3), as the number of methyl substituents increased from 0 to 5, the effect of illite varied from inhibition (0, 1, 2) to stimulation (3, 4) and then, to inhibition (5) (Figure S9). In general, with an increase in the number of methyl substituents, the steric hindrance, stability, and biodegradation resistance of naphthalene series compounds increase [64–67]. However, the effect of illite on the biodegradation of naphthalene series compounds was not consistent with this rule, and this phenomenon of altered influence with the increase in the methyl substitution number of naphthalene series was also exhibited by Mon [36] (Figure S14). The number of methyl substituents had a secondary effect when compared with the number of aromatic rings. For

example, in the three-ring phenanthrene series (Figure 3), the number of methyl substituents increased from 0 to 3, and the effect of illite on their biodegradation was consistently negative (Figure S10), which was different from that on the naphthalene series (Figure S9). In contrast, although the effect of Mon was positive, consistency in the biodegradation of different compounds in the phenanthrene series was also observed [29,30] (Figure S15).

Furthermore, the influence of illite on the biodegradation of AHs in *Pst*HO was affected by the connection mode of the aromatic rings. For instance, although both naphthalene series and biphenyl series have two aromatic rings (Figure 3), illite inhibited the biodegradation of monomethyl naphthalene and dimethyl naphthalene (Figure S9) but stimulated MeBph and dimethyl biphenyl biodegradation (Figure S12). The key difference between these two series is that the naphthalene series is formed by the fusion of two benzene rings, whereas the biphenyl series is formed by linking two phenyl groups through a single covalent bond (Figure 3).

The impact of illite on the biodegradation of AHs in *Pst*HO was affected by heteroatoms. In the fluorene series, fluorene (Fle), dibenzothiophene (DBT), and dibenzofuran (DBF) have the same structure, except that the atom at position 5 is carbon, sulfur, and oxygen, respectively (Figure 3). Illite had different effects on the biodegradation of these compounds, and it is inhibiting Fle biodegradation and stimulating DBT and DBF biodegradation (Figures 3 and S11). Similarly, this trend was also noted in the monomethyl substituents of these compounds, monomethyl fluorene, monomethyl dibenzothiophene, and monomethyl dibenzofuran (Figures 3 and S11). However, DBT exhibited the strongest biodegradation resistance, followed by Fle and DBF [64,68]. Thus, the influence of illite on AHs biodegradation was inconsistent with the biodegradation resistance of AHs. Larger sulfur and oxygen atoms, when compared with carbon atoms, can alter the polarity of the molecules, which might be the reason for the different effects of illite on these compounds. Illite had varied effects on compounds containing different heteroatoms in the fluorene series, unlike other clay minerals (modified or not) (Figure S16). Kao and Sap could inhibit the biodegradation of Fle and DBT (and their methyl or ethyl substituent), whereas Mon and Pal could stimulate their biodegradation [29,30,36] (Figure S16).

The influence of illite on the biodegradation of AHs in *Pst*HO was affected by the carbon chain length in the substituent. HRAHs have more than four rings (Figure 3; 72–96), and illite inhibited the biodegradation of HRAHs with no substituent or only one methyl substituent (Figure 3, 72–90; Figure S13), but stimulated the biodegradation of triaromatic steroid (TAS) (Figure 3; 91–96; Figure S13) with the longer carbon chain substituents (C2, C3, C8, C9, and C10). It must be noted that it is common for unmodified clay minerals, such as Mon, Kao, Sap, and Pal, to stimulate the biodegradation of TAS [30,36] (Figure S17).

The effect of illite on the biodegradation of AHs in *Pst*HO was not dominated by inhibition, as in the case of SHs. The positive effects of moderate SSA (and CEC) and weak local bridging effect were not sufficient to counteract the negative effects caused by adsorption, thus suggesting the possible occurrence of other positive mechanisms to explain the selective stimulation of illite to 45 AHs. Considering the facts that illite could not provide divalent cations (to form the local bridging effect) and this positive effect only occurred in AHs with π bonds, we speculated that the selective stimulation of illite was due to the cation-π [69] preferentially formed by monovalent cations and AHs with above five structure characteristics.

3.3. Kaolinization of Illite in P. stutzeri-Heavy Oil Complex

This study is the first to report the kaolinization of illite without smectite formation in illite-*Pst*HO. The XRD patterns of illite clay in P0I8 and unused samples were the same as the standard pattern (Figure 4a, ICDD PDF 26-0911 Illite), indicating that MVN and heavy oil L1YJC23 (including in situ microorganisms therein) did not change the crystal characteristics of illite in the absence of *P. stutzeri* (Figure 4a). Although the main characteristic peaks ($I_x/I_{max} \geq 0.5$) [70] of illite crystals still remained in the intermediate (formed in the process of kaolinization of illite) of P2I8, they were significantly weakened (e.g., (002),

(004), (006), and (136)) (Figure 4a). Other illite characteristic peaks ($I_x/I_{max} < 0.5$) [70] of the intermediate decreased ((025), (115), and (−116)) and disappeared ((−113), (023), (−114), and (114)) (Figure 4a). At the same time, the intermediate of P2I8 exhibited new characteristic peaks of Kao, such as (001), (002), (003), and (−113) (Figure 4a). Furthermore, the edges of the illite particles in P0I8 were sharp (Figure 4b), while those of the intermediate particles of P2I8 were round and had attached precipitates of 250–1000 nm (Figure 4c). This phenomenon of rounded edges (Figure 4c) caused by local dissolution is similar to the kaolinization of illite under abiotic condition [5]. After the destruction of the edges of the illite crystals, K^+ in the interlayers [71] was released to form cation-π [69], which stimulated the biodegradation of specific AHs. The organic products of biodegradation and ligands promoted the transformation of dissolved illite into the granular precipitate-aluminosilicate gel, which is considered the crucial first step in the two-step biological kaolinization [72]. The gel formed was deposited near the edges of the illite particles, which is considered to provide precursor materials and a crystallization environment for Kao. In the second step, biological metabolic activities further changed the local surrounding environment (pH, σ, and Eh) in and around the gel, resulting in the dissolution of the gel or rearrangement of its solid state to form Kao crystals [72]. Although previous studies have detected smectite (under the action of *Pseudogulbenkiania* sp.) in the process of kaolinization of illite [17,18], characteristic peaks of smectite were not observed in the present study, which may be attributed to the different microorganisms employed and the presence of heavy oil.

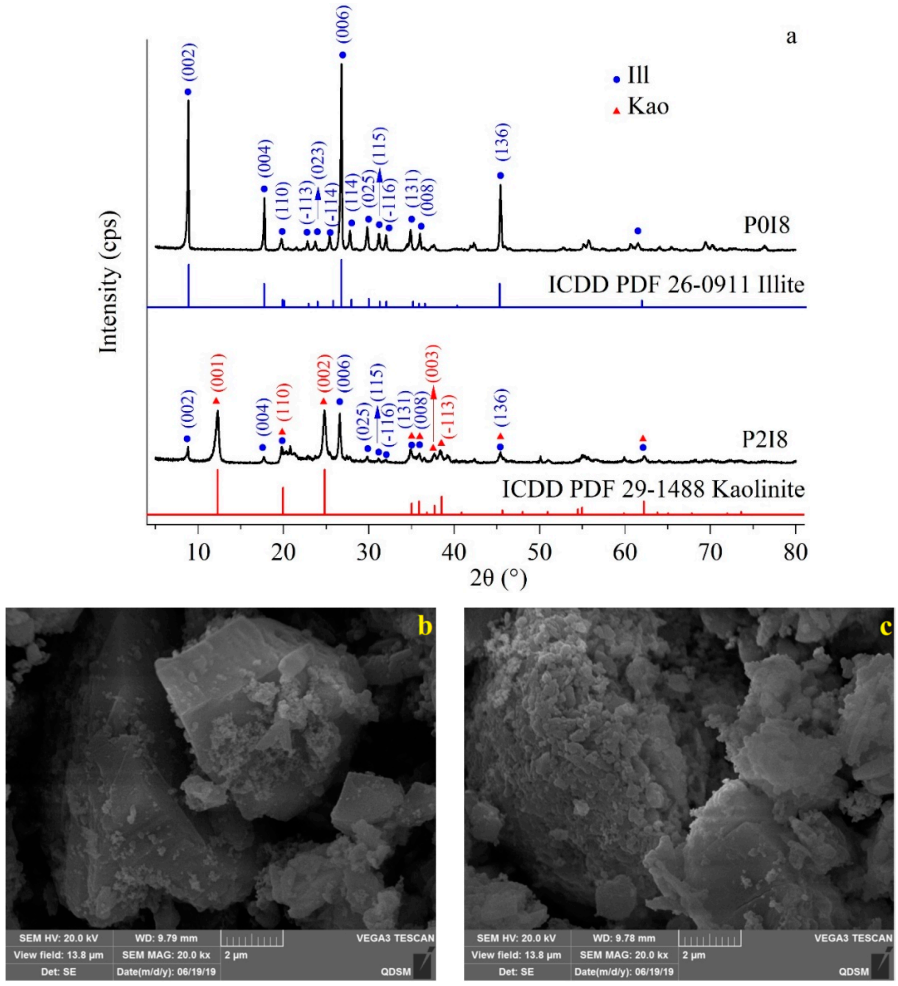

Figure 4. XRD (**a**) and SEM images (**b**,**c**) ((**b**) P0I8 and (**c**) P2I8) of the kaolinization in illite-*Pst*HO. Note: See Table 3 for P0I8 and P2I8; ICDD PDF 26-0911 and ICDD PDF 29-1488 represent the numbers of Powder Diffraction File, data source: International Centre for Diffraction Data (https://www.icdd.com, accessed on 12 October 2022).

4. Conclusions

To the best of our knowledge, this is the first report on the interaction of illite with the *Pst*HO complex. Although illite clay exerted a negative effect on the total heavy oil degradation ratio, it stimulated the biodegradation of 45 AHs in heavy oil, and its kaolinization in the illite-*Pst*HO was observed for the first time. The selective inhibition/stimulation effects of illite clay on biodegradation, as a supplementary mechanism of quasi-sequential and/or selective degradation, can be applied to protect high-quality SHs during microbial enhanced oil recovery process and remediation of specific AHs pollutant in polluted environments. Kaolinization of illite clay could be further explored to explain clay minerals transformations in oil reservoirs. For future study, new multivariate complex systems, such as illite-*Pst*HO could lead to richer discoveries in the field.

Supplementary Materials: The following supporting information can be downloaded at: https://www.mdpi.com/article/10.3390/microorganisms11020330/s1, Figure S1: Micrographs of cells of *Pseudomonas stutzeri* strain L1SHX-3X in an Eclipse Ni-U upright microscope (a) and a VEGA 3 SEM (b) after 6 days of reactivation by MVN-R from freeze-dried powder (storage at −80 °C) in the shaker with 120 rpm at 35 °C; Figure S2: Particle size distribution of illite measured by Mastersizer 3000; Figure S3: Genus-level analysis of in situ microorganisms in heavy oil L1YJC23; Figure S4: Difference in CO_2, O_2, and N_2 contents between illite-PstHO and atmosphere; Figure S5: *IND* of illite on biodegradation of SHs (a) and *RMC* of SHs (b) in the illite-PstHO; Figure S6: Total ion current diagrams of SHs in illite-PstHO after 56 days at 35 °C; Figure S7: *IND* of clay minerals on the biodegradation of SHs; Figure S8: Total ion current diagrams of AHs in the illite-PstHO after 56 days at 35 °C; Figure S9: *IND* of illite on the biodegradation of naphthalene series compounds (a) and *RMC* of naphthalene series compounds (b) in the illite-PstHO; Figure S10: *IND* of illite on the biodegradation of phenanthrene series compounds (a) and *RMC* of phenanthrene series compounds (b) in the illite-PstHO; Figure S11: *IND* of illite on the biodegradation of fluorene series compounds (a) and *RMC* of fluorene series compounds (b) in the illite-PstHO; Figure S12: *IND* of illite on biodegradation of biphenyl series compounds (a) and *RMC* of biphenyl series compounds (b) in the illite-PstHO; Figure S13: *IND* of illite on the biodegradation of HRAHs (a) and *RMC* of HRAHs (b) in the illite-PstHO; Figure S14: *IND* of clay minerals on the biodegradation of naphthalene series compounds; Figure S15: *IND* of clay minerals on the biodegradation of phenanthrene series compounds; Figure S16: *IND* of clay minerals on the biodegradation of fluorene series compounds; Figure S17: *IND* of clay minerals on the biodegradation of TAS; Table S1: The pH, σ and Eh of MVN and illite-PstHO; Table S2: Saturated hydrocarbons in heavy oil L1YJC23 and illite-PstHO detected by GC-MS; Table S3: Aromatic hydrocarbons in heavy oil L1YJC23 and illite-PstHO detected by GC-MS. References [23,25,29,30,36] are cited in the supplementary materials.

Author Contributions: Methodology, formal analysis, investigation, data curation, writing—original draft preparation, L.L.; Conceptualization, methodology, validation, formal analysis, resources, data curation, writing—review and editing, supervision, project administration, funding acquisition, Y.Y.W.; methodology, investigation, H.M.M.; methodology, S.B.S.; validation, resources, J.F.C. All authors have read and agreed to the published version of the manuscript.

Funding: This study was financially supported by the PetroChina Major Strategic Cooperation Projects (ZLZX2020010805, ZLZX2020020405), Forward Looking Foundation of China University of Pe-troleum-Beijing (ZX20190209), National Natural Science Foundation of China (41373086), National Science and Technology Major Project (2016ZX05050011, 2016ZX05040002), and Beijing Nova Program and Leading Talent Culturing Cooperative Projects (Z161100004916033).

Institutional Review Board Statement: Not applicable.

Informed Consent Statement: Not applicable.

Data Availability Statement: Data will be made available on request.

Acknowledgments: We sincerely appreciate Ji-Dong Gu for his proof reading and modification. Thank Liu Xiaoli and Luo Na for strains culturing, Liu Yuan for assisting in GC-MS data analysis. Thanks Zhang Yue for her high skills on the drawing of Orinin figures.

Conflicts of Interest: The authors declare that they have no conflict of interest.

References

1. Du, Q.; Sun, Z.; Forsling, W.; Tang, H. Adsorption of Copper at Aqueous Illite Surfaces. *J. Colloid Interface Sci.* **1997**, *187*, 232–242. [CrossRef] [PubMed]
2. Macht, F.; Eusterhues, K.; Pronk, G.J.; Totsche, K.U. Specific surface area of clay minerals: Comparison between atomic force microscopy measurements and bulk-gas (N2) and -liquid (EGME) adsorption methods. *Appl. Clay Sci.* **2011**, *53*, 20–26. [CrossRef]
3. Seabaugh, J.L.; Dong, H.; Kukkadapu, R.K.; Eberl, D.D.; Morton, J.P.; Kim, J. Microbial reduction of fe(III) in the Fithian and Muloorina illites: Contrasting extents and rates of bioreduction. *Clays Clay Miner.* **2006**, *54*, 67–79. [CrossRef]
4. Chang, P.-H.; Li, Z.; Jean, J.-S.; Jiang, W.-T.; Wang, C.-J.; Lin, K.-H. Adsorption of tetracycline on 2:1 layered non-swelling clay mineral illite. *Appl. Clay Sci.* **2012**, *67–68*, 158–163. [CrossRef]
5. Li, S.; He, H.; Tao, Q.; Zhu, J.; Tan, W.; Ji, S.; Yang, Y.; Zhang, C. Kaolinization of 2:1 type clay minerals with different swelling properties. *Am. Miner.* **2020**, *105*, 687–696. [CrossRef]
6. Sergeyev, Y.M.; Grabowska-Olszewska, B.; Osipov, V.I.; Sokolov, V.N.; Kolomenski, Y.N. The classification of microstructures of clay soils. *J. Microsc.* **1980**, *120*, 237–260. [CrossRef]
7. US Department of Interior and US Geological Survey. Heavy Oil and Natural Bitumen: Strategic Petroleum Resources. 2003; pp. 1–2. Available online: https://pubs.usgs.gov/fs/fs070-03/fs070-03.pdf (accessed on 12 December 2020).
8. Peters, K.E.; Walters, C.C.; Moldowan, J.M. *The Biomarker Guide: Biomarkers and Isotopes in Petroleum Exploration and Earth History*; Cambridge University Press: Cambridge, UK, 2005; pp. 560–579.
9. China National Energy Administration. *Classification of Oil Reservoir, SY/T6169-2021*; Petroleum Industry Press: Bijing, China, 2021. (In Chinese)
10. Rahman, P.; Thahira-Rahman, J.; Lakshmanaperumalsamy, P.; Banat, I. Towards efficient crude oil degradation by a mixed bacterial consortium. *Bioresour. Technol.* **2002**, *85*, 257–261. [CrossRef]
11. Nnabuife, O.O.; Ogbonna, J.C.; Anyanwu, C.; Ike, A.C.; Eze, C.N.; Enemuor, S.C. Mixed bacterial consortium can hamper the efficient degradation of crude oil hydrocarbons. *Arch. Microbiol.* **2022**, *204*, 306. [CrossRef]
12. Lalucat, J.; Bennasar, A.; Bosch, R.; Garcia-Valdes, E.; Palleroni, N.J. Biology of *Pseudomonas stutzeri*. *Microbiol. Mol. Biol. Rev.* **2006**, *70*, 510–547. [CrossRef]
13. Li, H.; Chen, G.; Zhang, Y.; Xu, H.; Jin, H.; Zhang, C. Isolation and identification of high-efficiency petroleum-degrading bacteria and their degradation characteristics. *J. Harbin Inst. Technol.* **2007**, *39*, 1664–1669. (In Chinese)
14. Celik, G.Y.; Aslim, B.; Beyatli, Y. Enhanced crude oil biodegradation and rhamnolipid production by *Pseudomonas stutzeri* strain G11 in the presence of Tween-80 and Triton X-100. *J. Environ. Biol.* **2008**, *29*, 867–870. [PubMed]
15. Hao, J.; Gao, L.; Wu, C.; Zhang, H.; Wang, Y.; Chen, Z.; Zhao, X. Isolation and optimization of a crude-oil-degrading bacteria *Pseudomonas stutzeri* TH-31. *Chin. J. Environ. Eng.* **2015**, *9*, 1771–1777.
16. Baquiran, J.P.; Thater, B.; Songco, K.; Crowley, D. Characterization of Culturable PAH and BTEX Degrading Bacteria from Heavy Oil of the Rancho La Brea Tarpits. *Polycycl. Aromat. Compd.* **2012**, *32*, 600–614. [CrossRef]
17. Zhao, L.; Dong, H.; Edelmann, R.E.; Zeng, Q.; Agrawal, A. Coupling of Fe(II) oxidation in illite with nitrate reduction and its role in clay mineral transformation. *Geochim. Cosmochim. Acta* **2017**, *200*, 353–366. [CrossRef]
18. Zhao, J.; Wu, W.; Zhang, X.; Zhu, M.; Tan, W. Characteristics of bio-desilication and bio-flotation of Paenibacillus mucilaginosus BM-4 on aluminosilicate minerals. *Int. J. Miner. Process.* **2017**, *168*, 40–47. [CrossRef]
19. Weise, A.M.; Lee, K. The effect of clay-oil flocculation on natural oil degradation. *Int. Oil Spill Conf. Proc.* **1997**, *1997*, 955–956. [CrossRef]
20. Chaerun, S.K.; Tazaki, K. How kaolinite plays an essential role in remediating oil-polluted seawater. *Clay Miner.* **2005**, *40*, 481–491. [CrossRef]
21. Chaerun, S.K.; Tazaki, K.; Asada, R.; Kogure, K. Interaction between clay minerals and hydrocarbon-utilizing indigenous microorganisms in high concentrations of heavy oil: Implications for bioremediation. *Clay Miner.* **2005**, *40*, 105–114. [CrossRef]
22. Warr, L.N.; Perdrial, J.N.; Lett, M.-C.; Heinrich-Salmeron, A.; Khodja, M. Clay mineral-enhanced bioremediation of marine oil pollution. *Appl. Clay Sci.* **2009**, *46*, 337–345. [CrossRef]
23. Froehner, S.; Da Luz, E.C.; Maceno, M. Enhanced Biodegradation of Naphthalene and Anthracene by Modified Vermiculite Mixed with Soil. *Water Air, Soil Pollut.* **2009**, *202*, 169–177. [CrossRef]
24. Ugochukwu, U.C.; Head, I.M.; Manning, D.A.C. Effect of modified montmorillonites on the biodegradation and adsorption of biomarkers such as hopanes, steranes and diasteranes. *Environ. Sci. Pollut. Res.* **2013**, *20*, 8881–8889. [CrossRef]
25. Ugochukwu, U.C.; Jones, M.D.; Head, I.M.; Manning, D.A.C.; Fialips, C.I. Biodegradation of crude oil saturated fraction supported on clays. *Biogeochemistry* **2013**, *25*, 153–165. [CrossRef] [PubMed]
26. Ugochukwu, U.C.; Manning, D.A.; Fialips, C.I. Microbial degradation of crude oil hydrocarbons on organoclay minerals. *J. Environ. Manag.* **2014**, *144*, 197–202. [CrossRef] [PubMed]
27. Ugochukwu, U.C.; Jones, M.D.; Head, I.M.; Manning, D.A.; Fialips, C.I. Effect of acid activated clay minerals on biodegradation of crude oil hydrocarbons. *Int. Biodeterior. Biodegrad.* **2014**, *88*, 185–191. [CrossRef]
28. Ugochukwu, U.C.; Jones, M.D.; Head, I.M.; Manning, D.A.; Fialips, C.I. Biodegradation and adsorption of crude oil hydrocarbons supported on "homoionic" montmorillonite clay minerals. *Appl. Clay Sci.* **2014**, *87*, 81–86. [CrossRef]

29. Ugochukwu, U.C.; Head, I.M.; Manning, D.A.C. Biodegradation and adsorption of C1- and C2-phenanthrenes and C1- and C2-dibenzothiophenes in the presence of clay minerals: Effect on forensic diagnostic ratios. *Biogeochemistry* **2013**, *25*, 515–527. [CrossRef]
30. Ugochukwu, U.C.; Manning, D.A.; Fialips, C.I. Effect of interlayer cations of montmorillonite on the biodegradation and adsorption of crude oil polycyclic aromatic compounds. *J. Environ. Manag.* **2014**, *142*, 30–35. [CrossRef]
31. Biswas, B.; Sarkar, B.; Mandal, A.; Naidu, R. Heavy metal-immobilizing organoclay facilitates polycyclic aromatic hydrocarbon biodegradation in mixed-contaminated soil. *J. Hazard. Mater.* **2015**, *298*, 129–137. [CrossRef]
32. Warr, L.N.; Friese, A.; Schwarz, F.; Schauer, F.; Portier, R.J.; Basirico, L.M.; Olson, G.M. Experimental study of clay-hydrocarbon interactions relevant to the biodegradation of the Deepwater Horizon oil from the Gulf of Mexico. *Chemosphere* **2016**, *162*, 208–221. [CrossRef]
33. Biswas, B.; Sarkar, B.; Naidu, R. Bacterial mineralization of phenanthrene on thermally activated palygorskite: A 14C radiotracer study. *Sci. Total Environ.* **2016**, *579*, 709–717. [CrossRef]
34. Biswas, B.; Sarkar, B.; Rusmin, R.; Naidu, R. Mild acid and alkali treated clay minerals enhance bioremediation of polycyclic aromatic hydrocarbons in long-term contaminated soil: A 14C-tracer study. *Environ. Pollut.* **2017**, *223*, 255–265. [CrossRef] [PubMed]
35. Ugochukwu, U.C.; Fialips, C.I. Removal of crude oil polycyclic aromatic hydrocarbons via organoclay-microbe-oil interactions. *Chemosphere* **2017**, *174*, 28–38. [CrossRef]
36. Ugochukwu, U.C.; Fialips, C.I. Crude oil polycyclic aromatic hydrocarbons removal via clay-microbe-oil interactions: Effect of acid activated clay minerals. *Chemosphere* **2017**, *178*, 65–72. [CrossRef] [PubMed]
37. Gong, B.; Wu, P.; Ruan, B.; Zhang, Y.; Lai, X.; Yu, L.; Li, Y.; Dang, Z. Differential regulation of phenanthrene biodegradation process by kaolinite and quartz and the underlying mechanism. *J. Hazard. Mater.* **2018**, *349*, 51–59. [CrossRef] [PubMed]
38. Warr, L.N.; Schlüter, M.; Schauer, F.; Olson, G.M.; Basirico, L.M.; Portier, R.J. Nontronite-enhanced biodegradation of Deepwater Horizon crude oil by Alcanivorax borkumensis. *Appl. Clay Sci.* **2018**, *158*, 11–20. [CrossRef]
39. Biswas, B.; Sarkar, B.; Faustorilla, M.V.; Naidu, R. Effect of surface-tailored biocompatible organoclay on the bioavailability and mineralization of polycyclic aromatic hydrocarbons in long-term contaminated soil. *Environ. Technol. Innov.* **2018**, *10*, 152–161. [CrossRef]
40. Tolpeshta, I.I.; Erkenova, M.I. Effect of Palygorskite Clay, Fertilizers, and Lime on the Degradation of Oil Products in Oligotrophic Peat Soil under Laboratory Experimental Conditions. *Eurasian Soil Sci.* **2018**, *51*, 229–240. [CrossRef]
41. Wang, G.F.; Wang, S.; Sun, W.; Zheng, S.L. Experimental Research on Bleaching of Illite by Acid Leaching. *Bull. Chin. Ceram. Soc.* **2016**, *35*, 1301–1305. (In Chinese)
42. Tian, Y.; Wan, Y.-Y.; Mu, H.-M.; Dong, H.-L.; Briggs, B.; Zhang, Z.-H. Microbial Diversity in High-Temperature Heavy Oil Reservoirs. *Geomicrobiol. J.* **2019**, *37*, 59–66. [CrossRef]
43. Mu, H.M.; Wan, Y.Y.; Wu, B.C.; Tian, Y.; Dong, H.L.; Xian, C.G.; Li, Y. A rapid change in microbial communities of the shale gas drilling fluid from 3548 m depth to the above-ground storage tank. *Sci. Total. Environ.* **2021**, *784*, 147009. [CrossRef]
44. Wan, Y.Y.; Dong, H. *Environmental Geomicrobiology Experiments*; Petroleum Industry Press: Beijing, China, 2014; pp. 100–105.
45. Van Niel, C.B. The culture, general physiology, morphology, and classification of the non-sulfur purple and brown bacteria. *Bacteriol. Rev.* **1944**, *8*, 1–118. [CrossRef] [PubMed]
46. Li, X.; Du, Y.; Wu, G.; Li, Z.; Li, H.; Sui, H. Solvent extraction for heavy crude oil removal from contaminated soils. *Chemosphere* **2012**, *88*, 245–249. [CrossRef]
47. Wan, Y.Y.; Du, W. *New Approach Technologies for Prevention and Control of Petroleum Contaminated and Sediments*; Petroleum Industry Press: Beijing, China, 2017; pp. 77–78.
48. Raheem, A.S.A.; Hentati, D.; Bahzad, D.; Abed, R.M.; Ismail, W. Biocatalytic upgrading of unconventional crude oil using oilfield-inhabiting bacterial consortia. *Int. Biodeterior. Biodegrad.* **2022**, *174*, 105468. [CrossRef]
49. Ransmark, E.; Svensson, B.; Svedberg, I.; Göransson, A.; Skoglund, T. Measurement of homogenisation efficiency of milk by laser diffraction and centrifugation. *Int. Dairy J.* **2019**, *96*, 93–97. [CrossRef]
50. *GB/T 30515-2014*; General Administration of Quality Supervision, Inspection and Quarantine of the People's Republic of China, 2014. Petroleum Products-Transparent and Opaque Liquids-Determination of Kinematic Viscosity and Calculation of Dynamic Viscosity. China Quality Inspection Press: Beijing, China, 2014. (In Chinese)
51. *GB/T 29617-2013*; General Administration of Quality Supervision, Inspection and Quarantine of the People's Republic of China, 2013. Determination of Density, Relative Density, and API Gravity of Iquids by Digital Density Meter. China Quality Inspection Press: Beijing, China, 2013. (In Chinese)
52. Goecks, J.; Nekrutenko, A.; Taylor, J. Galaxy the Galaxy Team Galaxy: A comprehensive approach for supporting accessible, reproducible, and transparent computational research in the life sciences. *Genome Biol.* **2010**, *11*, R86. [CrossRef]
53. Zhao, J.Y.; Li, L.; Wan, Y.Y.; Li, Z.G.; Luo, N.; Mu, H.M.; Li, W.H.; Zhang, Y. Interaction between in-situ oil reservoir microorganisms and minerals. *J. China Univ. Pet.* **2021**, *45*, 121–130. (In Chinese)
54. Du, W.D.; Wan, Y.Y.; Zhong, N.N.; Fei, J.J.; Zhang, Z.H. Current status of petroleum-contaminated soils and sediments. *J. Wuhan Univ.* **2011**, *57*, 311–322.
55. *SY/T5119-2016*; China National Energy Administration, 2016. Analysis Method for Family Composition of Rock Extracts and Crude Oil. Petroleum Industry Press: Beijing, China, 2013. (In Chinese)

56. Liu, Y.; Wan, Y.Y.; Zhu, Y.; Fei, C.; Shen, Z.; Ying, Y. Impact of Biodegradation on Polar Compounds in Crude Oil: Comparative Simulation of Biodegradation from Two Aerobic Bacteria Using Ultrahigh-Resolution Mass Spectrometry. *Energy Fuels* **2020**, *34*, 5553–5565. [CrossRef]
57. Gu, J.D. Biodegradation testing: So many tests but very little new innovation. *Appl. Environ. Biotechnol.* **2016**, *1*, 92–95. [CrossRef]
58. Liu, Y.; Wan, Y.Y.; Wang, C.; Ma, Z.; Liu, X.; Li, S. Biodegradation of n-alkanes in crude oil by three identified bacterial strains. *Fuel* **2020**, *275*, 117897. [CrossRef]
59. Kennedy, M.J.; Pevear, D.R.; Hill, R.J. Mineral Surface Control of Organic Carbon in Black Shale. *Science* **2002**, *295*, 657–660. [CrossRef] [PubMed]
60. Awad, A.M.; Shaikh, S.M.; Jalab, R.; Gulied, M.H.; Nasser, M.S.; Benamor, A.; Adham, S. Adsorption of organic pollutants by natural and modified clays: A comprehensive review. *Sep. Purif. Technol.* **2019**, *228*, 115719. [CrossRef]
61. Liu, J.; Xu, Z.; Masliyah, J. Role of fine clays in bitumen extraction from oil sands. *AIChE J.* **2004**, *50*, 1917–1927. [CrossRef]
62. Du, W.; Wan, Y.Y.; Zhong, N.N.; Fei, J.J.; Zhang, Z.H.; Chen, L.J.; Hao, J.M. Status quo of soil petroleum contamination and evolution of bioremediation. *Pet. Sci.* **2011**, *8*, 502–514. [CrossRef]
63. Wang, D.; Lin, J.; Lin, J.; Wang, W.; Li, S. Biodegradation of Petroleum Hydrocarbons by Bacillus subtilis BL-27, a Strain with Weak Hydrophobicity. *Molecules* **2019**, *24*, 3021. [CrossRef]
64. Volkman, J.K.; Alexander, R.; Kagi, R.I.; Rowland, S.J.; Sheppard, P.N. Biodegradation of aromatic hydrocarbons in crude oils from the Barrow Sub-basin of Western Australia. *Org. Geochem.* **1984**, *6*, 619–632. [CrossRef]
65. Fisher, S.J.; Alexander, R.; Kagi, R.I. Biodegradation of Alkylnaphthalenes in Sediments Adjacent to an Off-Shore Petroleum Production Platform. *Polycycl. Aromat. Compd.* **1996**, *11*, 35–42. [CrossRef]
66. Bao, J.; Zhu, C. The effects of biodegradation on the compositions of aromatic hydrocarbons and maturity indicators in biodegraded oils from Liaohe Basin. *Sci. China Ser. D Earth Sci.* **2009**, *52*, 59–68. [CrossRef]
67. van Aarssen, B.G.; Bastow, T.P.; Alexander, R.; Kagi, R.I. Distributions of methylated naphthalenes in crude oils: Indicators of maturity, biodegradation and mixing. *Org. Geochem.* **1999**, *30*, 1213–1227. [CrossRef]
68. Cheng, X.; Hou, D.; Mao, R.; Xu, C. Severe biodegradation of polycyclic aromatic hydrocarbons in reservoired crude oils from the Miaoxi Depression, Bohai Bay Basin. *Fuel* **2018**, *211*, 859–867. [CrossRef]
69. Zhu, D.; Herbert, B.E.; Schlautman, M.A.; Carraway, E.; Hur, J. Cation-π bonding: A new perspective on the sorption of polycyclic aromatic hydrocarbons to mineral surfaces. *J. Environ. Qual.* **2004**, *33*, 1322–1330. [CrossRef] [PubMed]
70. *SY/T5163-2018*; China National Energy Administration, 2018. Analysis Method for Clay Minerals and Ordinary Non-Clay Minerals in Sedimentary Rocks by the X-ray Diffraction. Petroleum Industry Press: Beijing, China, 2018. (In Chinese)
71. Hong, H.; Fang, Q.; Cheng, L.; Wang, C.; Churchman, G.J. Microorganism-induced weathering of clay minerals in a hydromorphic soil. *Geochim. Cosmochim. Acta* **2016**, *184*, 272–288. [CrossRef]
72. Fiore, S.; Dumontet, S.; Huertas, F.J.; Pasquale, V. Bacteria-induced crystallization of kaolinite. *Appl. Clay Sci.* **2011**, *53*, 566–571. [CrossRef]